Structural and kinetic mapping of side-chain exposure onto the protein energy landscape

Rachel Bernstein[a,b,1], Kierstin L. Schmidt[c,d,1], Pehr B. Harbury[d,2], and Susan Marqusee[b,e,2]

[a]Department of Chemistry, University of California, Berkeley, CA 94720; [b]Institute for Quantitative Biosciences (QB3), University of California, CA 94720; [c]Department of Chemistry, Stanford University, Stanford, CA 94305; [d]Department of Biochemistry, Stanford University School of Medicine, Stanford, CA 94305; and [e]Department of Molecular and Cell Biology, University of California, Berkeley, CA 94720

Identification and characterization of structural fluctuations that occur under native conditions is crucial for understanding protein folding and function, but such fluctuations are often rare and transient, making them difficult to study. Native-state hydrogen exchange (NSHX) has been a powerful tool for identifying such rarely populated conformations, but it generally reveals no information about the placement of these species along the folding reaction coordinate or the barriers separating them from the folded state and provides little insight into side-chain packing. To complement such studies, we have performed native-state alkyl-proton exchange, a method analogous to NSHX that monitors cysteine modification rather than backbone amide exchange, to examine the folding landscape of *Escherichia coli* ribonuclease H, a protein well characterized by hydrogen exchange. We have chosen experimental conditions such that the rate-limiting barrier acts as a kinetic partition: residues that become exposed only upon crossing the unfolding barrier are modified in the EX1 regime (alkylation rates report on the rate of unfolding), while those exposed on the native side of the barrier are modified predominantly in the EX2 regime (alkylation rates report on equilibrium populations). This kinetic partitioning allows for identification and placement of partially unfolded forms along the reaction coordinate. Using this approach we detect previously unidentified, rarely populated conformations residing on the native side of the barrier and identify side chains that are modified only upon crossing the unfolding barrier. Thus, in a single experiment under native conditions, both sides of the rate-limiting barrier are investigated.

intermediate | thiol exchange

In order to fold and function, proteins must explore structural fluctuations away from their native conformation. Such fluctuations result in a distribution of conformations of differing stabilities that, together with the barriers separating them, constitute the energy landscape. These high-energy partially unfolded forms are important for various biological functions, including allostery (1–3), catalysis (4), motions of motor proteins (5–7), and aggregation (8–10).

In spite of their importance, unfolding events occur very rarely under native conditions, and the populations of these conformations are very small, rendering experimental characterization of such partially unfolded species particularly challenging. Native-state amide hydrogen exchange (NSHX) has proven to be a powerful technique to identify and provide residue-specific structural information about such species (11). The power of NSHX to interrogate rare conformations is based on the Linderstrom-Lang model for the exchange process (12), where an amide hydrogen in the "closed" or native conformation must undergo a fluctuation to some alternative "open" conformation in order to exchange (Scheme 1). Because the majority of molecules are in the native conformation, they are not available for exchange, allowing for the detection of rare, high-energy "open" species.

Depending on the relative kinetics of these processes, the observed exchange rate (k_{obs}) can report on either the rate of forming the open state, k_{op} (EX1 regime, where $k_{cl} \ll k_{int}$), or

$$closed \underset{k_{cl}}{\overset{k_{op}}{\rightleftharpoons}} open \xrightarrow{k_{int}} exchanged$$

Scheme 1.

on the stabilities of open forms, K_{op} (EX2 regime, where $k_{cl} \gg k_{int}$) (13) (see *SI Text*). Under native conditions and at neutral pH, HX generally proceeds by the EX2 mechanism. Therefore, NSHX, which has successfully detected high-energy partially unfolded conformations in a number of proteins [see, for example, (14–21)], usually provides information only about the equilibrium populations of these species and not the barriers between them. Recently, methods employing triplet-triplet energy transfer have been used to probe both the kinetics and thermodynamics of extremely fast fluctuations on the native side of the rate-limiting barrier (22). Other studies have used a combination of EX1 and EX2 HX data to localize intermediates along the reaction coordinate (17, 20, 23–30). Although it is possible to access different regimes for different probes in a single HX experiment (31), such studies generally require probing the system under different experimental conditions, such as different pHs, and that these changes do not alter the protein's behavior.

Thiol alkyl-proton exchange (SX), which monitors cysteine side-chain modification, can access both the EX1 and EX2 regimes by simple adjustment of the concentration and chemical identity of the thiol-modifying reagent. Furthermore, under appropriately chosen experimental conditions, cysteine probes may kinetically partition into different exchange regimes, which allows localization of the associated exchange conformations on the reaction coordinate. For example, as shown in Fig. 1A, if the intrinsic thiol-modification rate is set such that global unfolding probes exhibit EX1 exchange kinetics, then so must all probes modified through a state on the unfolded side of the rate-limiting barrier. Moreover, the modification rates of such probes must match the rate of global unfolding. This tenet holds because all probe modification events are at least as fast as modification through the unfolded state, which itself is faster than recrossing the rate-limiting barrier from the unfolded side back to the native side. A corollary is that probes exhibiting EX2 exchange kinetics must be modified through states located on the native side of the rate-limiting barrier. It is also possible for probes modified on the native side to exhibit EX1 exchange kinetics, but such cases can be distinguished from unfolded-side probes because their rates of exchange will exceed the global unfolding rate. Thus the kinetic
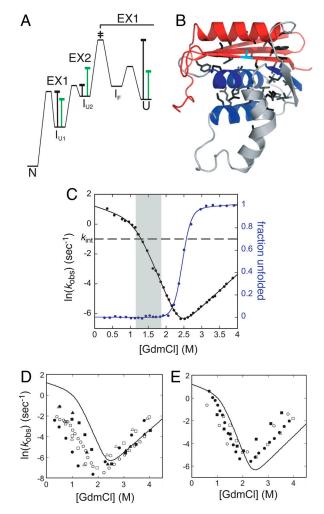
Fig. 1. Kinetic partitioning and D10A *E. coli* RNase H. (*A*) A model energy landscape showing the kinetic partitioning effect. Barrier heights are hypothetical and represented by vertical lines (black, conformational closing; green, intrinsic chemical modification). In this simple landscape, species on the unfolded side of the rate-limiting barrier exchange in EX1 and report on the global unfolding rate. Probes modified through fluctuations on the native side of the barrier may exchange in either EX1 or EX2. EX1 probes on the native side will be modified with rates faster than global unfolding. EX1 probes on each side of the transition state can therefore be distinguished by their observed kinetic behavior. (*B*) D10A *E. coli* RNase H. Positions investigated in NSSX experiments are shown as black sticks; Ala10 is shown in cyan sticks, and the backbone is colored according to the model of the NSHX PUF, with the structured region in blue and the unstructured in red. (*C*) CD-monitored GdmCl-induced equilibrium denaturation and folding and unfolding kinetics for D10A. The dashed line shows the intrinsic alkylation rate for 10 mM IAM, and the shaded region indicates [GdmCl] used for NSSX with EX1 probes. (*D*, *E*) CD-monitored folding and unfolding kinetics for EX1 (*D*) and a subset of the EX2 (*E*) probes; the fit of the D10A chevron is shown as a solid black line. (*D*) I7C, open circles; L49C, filled circles; I53C, filled squares; L56C, open squares; V65C, filled triangles; and L107C, open triangles. (*E*) Y22C, open circles; A55C, filled circles; A137C, filled squares; and A141C, open squares.

regime (EX1 or EX2) and exchange rate of each cysteine probe report on the position of its exchange state relative to the dominant feature in the energy landscape.

In addition to the flexibility of SX experiments to access kinetic exchange regimes denied to HX, SX also has the power to probe important side-chain packing interactions that can be invisible to HX experiments. This ability depends on the presence of cysteine residues, which presents a potential drawback, as such experiments are either limited to naturally occurring cysteines or require the introduction of nonnative cysteines that may result

in destabilization or changes to protein behavior. Thiol exchange, however, has been used to monitor the energetics of conformational changes such as unfolding (32–40), suggesting that the perturbing effect of cysteine substitutions can be overcome.

Here we carry out a detailed investigation of native-state alkyl-proton exchange (NSSX) for a large set of cysteine residues throughout a variant of *Escherichia coli* ribonuclease H (RNase H; Fig. 1*B*). This 155-amino acid protein is a well characterized model system known to populate a kinetic folding intermediate that resembles a high-energy conformation detected by NSHX (15, 41, 42). To expedite the SX characterization, we employ a modified version of Silverman's gel-based methodology to simultaneously monitor alkylation at multiple sites (43). The folding kinetics of the previously characterized variant D10A (44) relative to the intrinsic alkylation rate with the modifying agent iodoacetamide (IAM) allow us to apply a mixed EX1/EX2 approach to identify species on both sides of the rate-limiting barrier in a single experiment, characterize unique partially unfolded forms present on the folded side, and interrogate the rate-limiting folding barrier at the residue level.

Results and Discussion

Tuning Kinetics to Achieve EX1/EX2 Kinetic Partitioning. A version of the well characterized variant D10A *E. coli* RNase H* [*denotes a variant of the protein with the three native cysteines mutated to alanine (45)] suitable for our NSSX experiments was created by the addition of an N-terminal 6-His tag and a C-terminal ybbR tag for fluorescent labeling (46); this variant is referred to here simply as D10A. These tags do not affect the stability of RNase H* as measured by equilibrium GdmCl denaturation (Table S1). To explore the relative kinetics of D10A folding and alkylation, the folding and unfolding kinetics were determined by circular dichroism (CD). The resulting chevron plot reveals the characteristic rollover in the folding limb attributed to the presence of a folding intermediate, as expected based on previous folding studies of *E. coli* RNase H* variants carried out under slightly different conditions (44). The folding kinetics show that, under the conditions of the thiol exchange experiments for the slowest-exchanging probes ($\sim 1.2 - 1.8$ M GdmCl), k_{int} is slightly faster than k_f (Fig. 1*C*).

To determine the kinetic exchange regime for each probe, the dependence of the observed modification rates on the concentration of modifying reagent was measured; in EX2, the dependence is linear, while EX1 exchange is independent of modifying reagent concentration. Cysteine modification was detected by a scheme based on that originally used by Silverman (43) (Fig. 2). Briefly, pools of single-cysteine variants that were exposed to iodacetamide for various lengths of time were subsequently fluorescently labeled, denatured, cyanylated at unalkylated cysteines, and cleaved at the positions of cyanylation. Fragments were separated by gel electrophoresis and normalized fluorescent band intensities were fit to a three-parameter single exponential decay to yield an observed exchange rate.

Using this protocol, the kinetic exchange regime was characterized for 43 cysteine probes introduced by site-directed mutagenesis into the D10A background (Fig. 3 *A* and *B*, Table 1). Seven probes exchanged in the EX1 regime and 19 in the EX2 regime, demonstrating that successful kinetic tuning had been achieved. Five probes exchanged by a mixture of EX1 and EX2 termed EXX (47), indicating that the closing rate for these probes is approximately the same as the intrinsic alkylation rate, and 12 exchanged too quickly to measure.

The perturbing effect of introducing cysteine mutations was investigated by determining the ΔG°_{unf} with CD-monitored GdmCl-induced denaturation for 18 single-cysteine variants in the D10A background. Destabilization due to the cysteine mutations varied ($\Delta\Delta G^{\circ} = 0.2 - 4.4$ kcal/mol) (Table S1), indicating that caution must be used when interpreting the site-
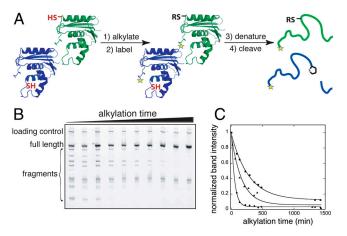
Fig. 2. A schematic diagram of the NSSX experiment. (*A*) Single-cysteine variants are pooled and exposed to a thiol-reactive modifying agent; buried thiols (blue protein) are alkylated less quickly than exposed thiols (green protein). Proteins are then fluorescently labeled at the C-terminal peptide tag, unfolded, and exposed to the cyanylating agent NTCB. Previously unreacted cysteines are cyanylated and cleaved upon pH increase, while modified cysteines do not react with NTCB and thus are not cleaved. (*B*) Peptide fragments are resolved using a high-resolution polyacrylamide gel and band intensities are normalized based on a loading control and fit to a single exponential. (*C*) Representative traces for the Y22C probe at multiple [GdmCl] (squares, 0.71 M; triangles, 1.09 M; and circles, 1.30 M); alkylation rates increase with increasing [GdmCl].

specific energetics determined by SX. Kinetic folding/unfolding experiments monitored by CD were also conducted with a subset of the single-cysteine variants (Fig. 1 *D* and *E*). The EX1 probes show slower folding than the D10A parent protein, while the unfolding rates are relatively unchanged (Fig. 1*D*), indicating that the side chains at these positions are involved in the rate-limiting transition state to folding, as suggested by our kinetic partition model. In contrast, the EX2 probes show faster unfolding but do not significantly affect the folding rate (Fig. 1*E*), indicating that the interactions involving these side chains are formed after the protein has traversed the major barrier to folding, which is also consistent with our model. Thus, the introduced mutations affect folding kinetics in a way that reinforces rather than invalidates the kinetic partition scheme.

Having identified suitable conditions where probes partition between EX1 and EX2 kinetics and defined a range of kinetic and equilibrium effects due to the cysteine mutations, NSSX (thiol reactivity as a function of [GdmCl]) was carried out on D10A. The following analysis focuses only on probes that reacted by either EX1 or EX2 kinetics; due to the complexity of interpreting the exchange behavior for EXX probes, they were omitted from further structural interpretation.

EX1 Probes Reveal Information About Early Events in Folding. Under the conditions of our experiment, we expect that all modification on the unfolded side of the barrier, either from an intermediate or from the unfolded state, should exhibit EX1 kinetics. The rate of modification for unfolded-side probes should then correspond to the global unfolding rate. As expected, the EX1 alkylation rates observed under the conditions of our experiment agree with the expected global unfolding rate as determined by CD (Fig. 3*C*). A linear extrapolation to 0 M GdmCl, however, yields a range of $k_{op}(H_2O)$ from about 10^{-6} sec^{-1} to 10^{-8} sec^{-1}, mostly due to variation in the calculated slopes, or *m*-values (Table 1). Similar variation in the opening rates determined by HX has been seen for the protein turkey ovomucoid third domain and interpreted as independent unfolding events (23). It is unclear, however, whether the distribution seen in these NSSX experiments represents a real distribution in residue-specific opening rates, a result
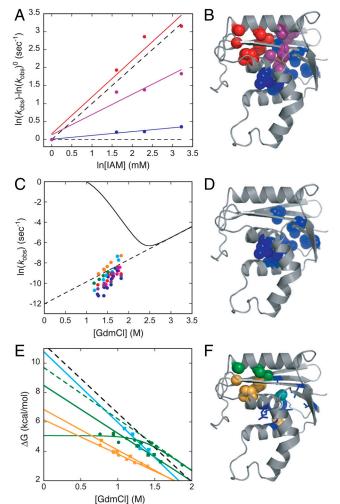

Fig. 3. NSSX data and results. (*A*) The kinetic exchange regime was determined for all probes; a representative sample at 1.4 M GdmCl is shown (A137C, red; I25C, purple; and L107C, blue). The dashed line with no slope represents expected EX1 behavior and the dashed line with unity slope shows expected EX2 behavior. (*B*) D10A with NSSX probes colored according to their kinetic exchange regime (EX1, blue; EX2, red; and EXX, purple). Positions that exchange fast or with fluctuations are not shown. (*C*) Alkylation rates for EX1 probes plotted as a function of [GdmCl] relative to the fit of the CD chevron (I7C, red; A24C, pink; L49C, green; I53C, blue; L56C, cyan; V65C, purple; and L107C, orange); the dashed line is the extrapolation of the chevron unfolding limb. The error for the fit of the exponential decay for each point is at most ±0.5 ln(k_{obs}), with an average error of ±0.2 ln(k_{obs}). (*D*) EX1 probes, shown in blue spheres, are mostly in the protein core. (*E*) Representative samples of denaturant-dependent EX2 probes, colored by PUFs as designated in Table 1 (G20C, yellow circles; M47C, yellow squares; A137C, green squares; A141C, green circles; and A55C, cyan squares). The green dashed line reflects a linear extrapolation of the denaturant-dependent exchange region for a probe with denaturant-independent exchange at low [GdmCl]. The black dashed line is an extrapolation of the kinetic ΔG and *m*-value as measured by CD. The error for the fit of the exponential decay for each point is at most ±0.3 kcal/mol, with an average error of ±0.15 kcal/mol. (*F*) PUFs as represented by SX probes rendered in spheres: green, helix E PUF; yellow, clamshell PUF; and cyan, high-energy PUF. EX1 probes are shown as blue sticks.

of small changes due to the effect of the cysteine substitution, or simply noise in the data.

Most of the probes that show EX1 behavior reside in the core of the protein (Fig. 3*D*), identified both as an early protected region (<10 msecs) in pulse-labeling HX studies (41) and an equilibrium intermediate by NSHX (15, 42). The exchange behavior of these probes indicates that, as expected, this core region is not modified upon fluctuations on the native side of the barrier, and

Table 1. NSSX results

Position	Secondary structure	Behavior	$\ln(k_{obs})$ (H$_2$O)	$\Delta G°_{SX}$ (kcal/mol)	m-value (kcal/mol M^{-1})	$\Delta G°_{fluc}$ (kcal/mol)
I7	strand 1	EX1	−14.3 ± 0.6		1.8 ± 0.4	
F8	strand 1	fast				
T9	strand 1	EXX				
G11	strand 1	fast				3.4 ± 0.5
S12	strand 1	EX2				3.5 ± 0.2
G20	strand 2	EX2		6.2 ± 0.4	2.3 ± 0.3	
G21	strand 2	fast				
Y22	strand 2	EX2		8.1 ± 0.6	3.0 ± 0.5	
G23	strand 2	EX2		10.6 ± 0.6	3.6 ± 0.4	
A24	strand 2	EX1	−18.2 ± 1.0		3.2 ± 0.6	
I25	strand 2	EXX				
S36	strand 3	fast				
A37	strand 3	EX2				3.1 ± 0.3
Y39	strand 3	fast				
M47	helix A	EX2		6.7 ± 0.3	2.7 ± 0.2	
L49	helix A	EX1	−14.0 ± 1.1		2.0 ± 0.8	
A51	helix A	EXX				
A52	helix A	EXX				
I53	helix A	EX1	−17.0 ± 0.8		2.7 ± 0.4	
V54	helix A	EX2				2.9 ± 0.3
A55	helix A	EX2		10.3 ± 0.7	4.4 ± 0.5	
L56	helix A	EX1	−17.4 ± 0.6		3.3 ± 0.4	
L59	helix A	EX2				3.0 ± 0.2
V65	strand 4	EX1	−14.7 ± 0.7		2.0 ± 0.4	
L67	strand 4	EX2				3.3 ± 0.1
S68	strand 4	EX2				4.3 ± 0.3
V74	helix B	EX2				4.4 ± 0.4
R75	helix B	EX2				2.6 ± 0.2
I78	helix B	EX2				3.6 ± 0.3
I82	helix C	fast				
L103	helix D	EX2				2.3 ± 0.1
R106	helix D	fast				
L107	helix D	EX1	−13.4 ± 0.7		2.0 ± 0.5	
A110	helix D	EX2		8.8 ± 0.6	2.4 ± 0.4	
H114	loop	fast				
I116	strand 5	EX2				4.9 ± 0.4
V121	strand 5	fast				
E129	helix E	fast				
N130	helix E	fast				
A133	helix E	EXX				
L136	helix E	fast				
A137	helix E	EX2		8.8 ± 0.4	3.5 ± 0.3	
A141	helix E	EX2		9.7 ± 0.8	3.5 ± 0.5	5.1 ± 0.1

Error propagated using average error for each point and overall error of the fit. $\Delta G°_{fluc}$ calculated assuming m-value of 0.

the protein must completely unfold for chemical modification of these sites at both the side-chain and backbone level.

Two EX1 probes, I7C and A24C, fall outside the core as previously defined by HX experiments. Our model, based on both pulse-labeling and native-state hydrogen exchange data, suggests that these residues are exposed in the folding intermediate. There were no data, however, to indicate where on the folding trajectory these residues become protected. These probes' NSSX EX1 behavior and observed alkylation rates, which match those for the other EX1 probes, suggest that these two side chains only become exposed and available for modification on the unfolded side of the barrier. For further confirmation, we measured the effects of the cysteine substitution on the folding kinetics. While A24C has no effect, the I7C mutation slows folding (Fig. S1), and analysis of the kinetic effect indicates that the side chain gains structure on the unfolded side of the barrier, primarily after formation of the intermediate but before the transition state [$\Phi^I = 0.3$, $\Phi^\ddagger = 1.2$ (Table S2)]. Thus, modification of I7C likely occurs on the unfolded side of the barrier. The side chains of I7 and A24 are directed toward the core region, consistent with the suggestion that both are involved in important, previously unidentified packing interactions that stabilize the transition state.

EX2 Probes Explore Ruggedness of the Native Side of the Barrier.

For those probes that were modified by EX2 kinetics, the observed alkylation rates were converted to free energies ($\Delta G°_{SX}$) and plotted as a function of [GdmCl] (Fig. 3E). As seen in similar native-state hydrogen exchange experiments, these data revealed both denaturant-dependent and denaturant-independent behavior (15, 34, 42). All but one of the SX probes displayed only one of these mechanisms and thus could be fit linearly (A141C required a more complex fit to accommodate both types of alkylation) (see SI Text). The resulting m-values and extrapolated $\Delta G°_{SX}$(H$_2$O) and $\Delta G°_{fluc}$ are shown in Table 1. Eleven of the EX2 probes, all of which reside near the surface of the protein, show alkylation rates with no or low denaturant dependence (m-value <1.4); modification at these positions was thus attributed to local structural fluctuations. Exchange of one additional probe, G11C, was also attributed to local structural fluctuations, but reacted too quickly under the conditions used for kinetic regime testing to confirm whether its exchange occurred by EX2. The remaining eight EX2 probes had denaturant-dependent alkylation rates, suggesting unfolding events that expose specific regions of the protein, or so-called partially unfolded forms (PUFs). The variation in destabilizing effects of the cysteine mutations prohibits our use of the $\Delta G°_{SX}$(H$_2$O) as a criterion to cluster these probes into PUFs; instead, probes were grouped based on their calculated m-values and structural relationships, resulting in three clusters (Fig. 3F, Table 2).

The PUF with an intermediate m-value (Fig. 3F, green spheres) consists of side chains that reside on or pack with the final helix of the protein, the E helix. These probes would be exposed in a conformation with the E helix either undocked or unfolded, whose existence has been suggested by several independent lines of evidence. A fragment without the E helix shows cooperative folding and the ability to bind a peptide corresponding to the E helix (48), and NSHX on *Thermus thermophilus* RNase H, a thermophilic homolog of the *E. coli* protein, revealed a PUF corresponding to the unfolding of this helix (49).

These thiol exchange suggest the presence of this intermediate in full-length *E. coli* RNase H, which was not seen in previous NSHX experiments with either the wild-type or D10 variant, perhaps because they were limited to the EX2 regime (15, 42). The hydrogen exchange results reveal the lowest energy PUF involving the E helix, and under the conditions of that experiment, the E helix exchanges from a conformation whose structure correlates with the folding intermediate, with both the E helix and the β sheet unfolded. The conformation suggested by these thiol exchange experiments, with the E helix exposed on the native side of the barrier, would be missed in the NSHX experiments if it were higher in energy than the folding intermediate. Because in our NSSX experiments the well characterized folding intermediate is accessed more slowly (EX1) than the native-side PUF (EX2), we are able to detect the PUF.

Table 2. EX2 probe clustering

Cluster	Position	$\Delta G°_{SX}$ (kcal/mol)	m-value (kcal/mol M^{-1})
Yellow	G20	6.2 ± 0.3	2.3 ± 0.5
	Y22	8.1 ± 0.6	3.0 ± 0.5
	M47	6.7 ± 0.3	2.7 ± 0.2
	A110	8.8 ± 0.6	2.4 ± 0.4
	average	**7.5 ± 0.6**	**2.6 ± 0.5**
Green	G23	10.6 ± 0.6	3.6 ± 0.4
	A137	8.8 ± 0.4	3.5 ± 0.3
	A141	9.7 ± 0.8	3.5 ± 0.5
	average	**9.7 ± 0.8**	**3.5 ± 0.5**
Cyan	A55	10.3 ± 0.7	4.4 ± 0.5

Errors for averages are standard deviations.

The denaturant dependence, or *m*-value, for this unfolding intermediate of 3.5 kcal/mol·M as measured by thiol exchange is quite high relative to the *m*-values of 5.0 kcal/mol·M for global unfolding (equilibrium denaturation monitored by CD; Table S1), 1.3 kcal/mol·M for unfolding from the native state to the transition state, and 1.8 kcal/mol·M for N to the folding intermediate (CD-monitored kinetics; Table S2). Such unexpectedly high *m*-values are also seen for the other EX2 probes. If these *m*-values determined by our thiol exchange studies correspond to changes in exposed surface area, the data present a paradox: native-side PUFs that are more solvent-exposed than the transition state for unfolding. This interpretation would suggest either that *m*-value is not a good model for progress along the unfolding reaction coordinate, or that we have identified off-pathway intermediates with high degrees of solvent-exposed surface area.

Interestingly, NSHX-monitored unfolding of helix E and the β sheet of RNase H D10A also exhibits an *m*-value of about 3.5 (42). One possible explanation for our data is that, although the probes that define this PUF are located along the E helix interface, the structure of this PUF corresponds to unfolding of more than just that helix. In such a scenario, the native-state thiol exchange experiments may access a native-side PUF with the E helix and β sheet unfolded. An alternative explanation is that the free energies derived from these thiol-modification rates increase with denaturant concentration independently of changes in solvent-exposed surface area. If this model holds, our analysis would lead to anomalously high *m*-values (and corresponding $\Delta G°_{SX}$) unrelated to protein conformational change. This interpretation would also explain the cases where $\Delta G°_{SX} \geq \Delta G°_{Gdm\ melt}$, though this difference in $\Delta G°$, most notably seen for G23C, could also be the result of a PUF that is higher in energy than the unfolded state.

A second PUF consists primarily of side chains at the interface of helix A and strand 2 (Fig. 3*F*, yellow spheres). The smaller *m*-values for these probes (m_{avg} = 2.6 kcal/mol·M) suggest less exposure of nonpolar surface area in this PUF, perhaps indicating an intermediate formed by a clamshell-like motion in which the β sheet and E helix move up and away from the core helices without unfolding. HX experiments do not reveal any such motion, likely due to the fact that this conformation exposes side chains while retaining the backbone hydrogen-bond network. Furthermore, the side chains exposed in the yellow PUF are proximal to the active site, suggesting that this species may be important for enzymatic activity. Detection of this clamshell-like motion highlights the ability of SX to provide important insights by probing side-chain packing.

The final PUF consists of a single probe, A55C, at the end of helix A (Fig. 3*F*, cyan spheres). This probe resides within the core region as defined by backbone NSHX and is modified with a $\Delta G°_{SX}$ and *m*-value close to those associated with global unfolding. There have been previous examples of single point mutations changing the exchange regime (50, 51); however, the measured CD kinetics show little change in the folding limb, suggesting that this is not the case (Fig. 1*E*). Thus, it appears that alkylation at this position does not require crossing the rate-limiting folding barrier, indicating that A55C is exposed in a high-energy fluctuation on the folded side of the barrier. It is difficult, however, to construct a structural model for this species based on a single probe. Similarly, A110C showed analogous behavior to the yellow PUF, but because of its distant location at the end of helix D, this probe was omitted from structural interpretation.

Thiol Alkylation Provides Information About Side-Chain Packing.
These SX experiments highlight the importance of side-chain interactions in folding. The EX1 kinetics that report on the global unfolding rate at positions 7 and 24, in conjunction with the Φ-value analysis for I7C, indicate that, during folding, these side chains become structured prior to the rate-limiting transition

state, earlier than detected by previous kinetic HX experiments. The clamshell-like (yellow) PUF suggests a species, potentially involved in activity, that does not involve any change in backbone hydrogen bonding, and there are likely similar motions in other systems that are important for activity but are largely invisible to HX experiments due to an absence of associated backbone perturbations. Furthermore, analyses of the positions that react by fluctuations (independent of [GdmCl]) or are alkylated too quickly to measure provide additional evidence of variation between side chain and backbone exchange behavior. There are many instances where the side chain is exposed to solvent while the backbone is protected, but there are also four probes (L49C, I116C, A133C, and A137C) that show protection by SX despite exchanging too quickly to measure by HX. These probes do not describe a structurally contiguous region, but their SX behavior indicates that side chains can play a crucial role in anchoring different regions of the protein, even while the backbone is subject to fluctuations.

The nature of intermediates on the native side of the unfolding barrier has been a topic of recent interest. There is some evidence that unfolding begins with the formation of a dry molten globule (22, 52). While the intermediates we observe may be related to such a dry molten globule, our data only provide information about side chain exposure that allows for alkylation by iodoacetamide. Thus, further experiments are needed to test if any of these newly identified intermediates on the native side of the barrier arise from fluctuations involving a dry molten globule state. For example, Loh and coworkers (53) have shown that SX experiments carried out with thiol-modifying reagents of different sizes can yield information about the magnitude of opening events that expose specific thiol groups; such experiments may provide useful insight into the nature of the species detected here.

Conclusions
Native-state alkyl-proton exchange offers a powerful complement to hydrogen exchange studies of a protein's energy landscape. In addition to providing information about the environment of the side chain, SX provides the opportunity to obtain both kinetic (EX1) and thermodynamic (EX2) information under the same conditions (pH, temp, etc). By tuning the intrinsic thiol-alkylation rate and using a well characterized variant of *E. coli* RNase H, we have assigned probes to alkylation-competent species on either side of the barrier. Furthermore, these SX experiments identify PUFs on the folded side of the barrier that in NSHX may have been masked by the lack of backbone exposure or the limitations of an all-EX2 equilibrium experiment.

As a general tool, the approach of a mixed EX1/EX2 thiol exchange experiment has a number of advantages over a traditional EX2 experiment. The ability to assign species to specific regions of the reaction coordinate relative to the rate-limiting barrier is of paramount importance for characterizing folding and unfolding pathways. The kinetic partitioning principle can also be extended by taking advantage of the range of intrinsic rates furnished by a variety of modification agents to explore specific regions of the landscape based on different kinetic barriers. The ability of these NSSX experiments to detect high-energy species on the folded side of the rate-limiting barrier, even if the same positions are also exposed in lower energy species on the other side of the barrier, provides an important tool for identification of partially unfolded forms. Furthermore, SX experiments reveal unique information about the role of side-chain packing in folding that is not revealed by HX. Finally, by combining HX and SX experiments to access different kinetic regimes and probe backbone vs. side-chain exchange, we can create a more complete picture of the protein's energy landscape than either technique can provide alone.

Materials and Methods

Gene and Protein Construction. An N-terminal 6-His tag and a C-terminal ybbR tag (46) were added to the gene encoding the D10A *E. coli* RNase H* variant (44). Individual cysteine mutations were introduced by Quik-Change mutagenesis. Protein variants were expressed and purified in mixed pools as described in *SI Text*.

Thiol Exchange. Pools of single-site cysteine mutants were grown and purified in eight bins. Thiol exchange experiments were conducted in 100 mM bicine pH 8.6, 50 mM KCl, 1 mM tris(2-carboxyethyl)phosphine (TCEP). CD experiments were conducted in 20 mM Tris pH 8.6, 50 mM KCl, and 0.1 mM TCEP for single-cysteine mutants. Thiol-alkylation studies were analyzed using the classic EX1/EX2 formalism applied to hydrogen exchange (see *SI Text*). To determine the kinetic exchange regime, pools of cysteine-containing D10A variants were incubated with 1, 5, 10, and 25 mM IAM at 1.4 and 1.8 M GdmCl; alkylation was quenched at various time points with an excess of DTT. Probes with slopes below 0.25 were classified as EX1, slopes above 0.7 EX2, and slopes between 0.5–0.6 EXX. Subsequent NSSX experiments were conducted in an analogous method by measuring alkylation rates as a function of [GdmCl] using 10 mM IAM.

1. Miyashita O, Onuchic JN, Wolynes PG (2003) Nonlinear elasticity, proteinquakes, and the energy landscapes of functional transitions in proteins. *Proc Natl Acad Sci USA* 100:12570–12575.
2. Schrank TP, Bolen DW, Hilser VJ (2009) Rational modulation of conformational fluctuations in adenylate kinase reveals a local unfolding mechanism for allostery and functional adaptation in proteins. *Proc Natl Acad Sci USA* 106:16984–16989.
3. Tripathi S, Portman JJ (2009) Inherent flexibility determines the transition mechanisms of the EF-hands of calmodulin. *Proc Natl Acad Sci USA* 106:2104–2109.
4. Bemporad F, et al. (2008) Biological function in a non-native partially folded state of a protein. *EMBO J* 27:1525–1535.
5. Terada TP, Sasai M, Yomo T (2002) Conformational change of the actomyosin complex drives the multiple stepping movement. *Proc Natl Acad Sci USA* 99:9202–9206.
6. Hyeon C, Onuchic JN (2007) Mechanical control of the directional stepping dynamics of the kinesin motor. *Proc Natl Acad Sci USA* 104:17382–17387.
7. Hyeon C, Onuchic JN (2007) Internal strain regulates the nucleotide binding site of the kinesin leading head. *Proc Natl Acad Sci USA* 104:2175–2180.
8. Booth DR, et al. (1997) Instability, unfolding and aggregation of human lysozyme variants underlying amyloid fibrillogenesis. *Nature* 385:787–793.
9. Khurana R, et al. (2001) Partially folded intermediates as critical precursors of light chain amyloid fibrils and amorphous aggregates. *Biochemistry* 40:3525–3535.
10. Quintas A, Vaz DC, Cardoso I, Saraiva MJ, Brito RM (2001) Tetramer dissociation and monomer partial unfolding precedes protofibril formation in amyloidogenic transthyretin variants. *J Biol Chem* 276:27207–27213.
11. Bai Y (2006) Protein folding pathways studied by pulsed- and native-state hydrogen exchange. *Chem Rev* 106:1757–1768.
12. Berger A, Linderstrom-Lang K (1957) Deuterium exchange of poly-DL-alanine in aqueous solution. *Arch Biochem Biophys* 69:106–118.
13. Hvidt A, Nielsen SO (1966) Hydrogen exchange in proteins. *Adv Protein Chem* 21:287–386.
14. Bai Y, Sosnick TR, Mayne L, Englander SW (1995) Protein folding intermediates: native-state hydrogen exchange. *Science* 269:192–197.
15. Chamberlain AK, Handel TM, Marqusee S (1996) Detection of rare partially folded molecules in equilibrium with the native conformation of RNaseH. *Nat Struct Biol* 3:782–787.
16. Fuentes EJ, Wand AJ (1998) Local dynamics and stability of apocytochrome b562 examined by hydrogen exchange. *Biochemistry* 37:3687–3698.
17. Yan S, Kennedy SD, Koide S (2002) Thermodynamic and kinetic exploration of the energy landscape of Borrelia burgdorferi OspA by native-state hydrogen exchange. *J Mol Biol* 323:363–375.
18. Krishna MM, Lin Y, Rumbley JN, Englander SW (2003) Cooperative omega loops in cytochrome c: role in folding and function. *J Mol Biol* 331:29–36.
19. Maity H, Maity M, Krishna MM, Mayne L, Englander SW (2005) Protein folding: the stepwise assembly of foldon units. *Proc Natl Acad Sci USA* 102:4741–4746.
20. Bollen YJ, Kamphuis MB, van Mierlo CP (2006) The folding energy landscape of apoflavodoxin is rugged: hydrogen exchange reveals nonproductive misfolded intermediates. *Proc Natl Acad Sci USA* 103:4095–4100.
21. Vadrevu R, Wu Y, Matthews CR (2008) NMR analysis of partially folded states and persistent structure in the alpha subunit of tryptophan synthase: implications for the equilibrium folding mechanism of a 29-kDa TIM barrel protein. *J Mol Biol* 377:294–306.
22. Reiner A, Henklein P, Kiefhaber T (2010) An unlocking/relocking barrier in conformational fluctuations of villin headpiece subdomain. *Proc Natl Acad Sci USA* 107:4955–4960.
23. Arrington CB, Robertson AD (1997) Microsecond protein folding kinetics from native-state hydrogen exchange. *Biochemistry* 36:8686–8691.
24. Sivaraman T, Arrington CB, Robertson AD (2001) Kinetics of unfolding and folding from amide hydrogen exchange in native ubiquitin. *Nat Struct Biol* 8:331–333.
25. Hoang L, Bedard S, Krishna MM, Lin Y, Englander SW (2002) Cytochrome c folding pathway: kinetic native-state hydrogen exchange. *Proc Natl Acad Sci USA* 99:12173–12178.
26. Rodriguez HM, Robertson AD, Gregoret LM (2002) Native state EX2 and EX1 hydrogen exchange of *Escherichia coli* CspA, a small beta-sheet protein. *Biochemistry* 41:2140–2148.
27. Cliff MJ, Higgins LD, Sessions RB, Waltho JP, Clarke AR (2004) Beyond the EX1 limit: probing the structure of high-energy states in protein unfolding. *J Mol Biol* 336:497–508.
28. Schanda P, Forge V, Brutscher B (2007) Protein folding and unfolding studied at atomic resolution by fast two-dimensional NMR spectroscopy. *Proc Natl Acad Sci USA* 104:11257–11262.
29. Bedard S, Mayne LC, Peterson RW, Wand AJ, Englander SW (2008) The foldon substructure of staphylococcal nuclease. *J Mol Biol* 376:1142–1154.
30. Wani AH, Udgaonkar JB (2009) Native state dynamics drive the unfolding of the SH3 domain of PI3 kinase at high denaturant concentration. *Proc Natl Acad Sci USA* 106:20711–20716.
31. Yi Q, Baker D (1996) Direct evidence for a two-state protein unfolding transition from hydrogen-deuterium exchange, mass spectrometry, and NMR. *Protein Sci* 5:1060–1066.
32. Ha JH, Loh SN (1998) Changes in side chain packing during apomyoglobin folding characterized by pulsed thiol-disulfide exchange. *Nat Struct Biol* 5:730–737.
33. Feng Z, Butler MC, Alam SL, Loh SN (2001) On the nature of conformational openings: native and unfolded-state hydrogen and thiol-disulfide exchange studies of ferric aquomyoglobin. *J Mol Biol* 314:153–166.
34. Silverman JA, Harbury PB (2002) The equilibrium unfolding pathway of a (beta/alpha)8 barrel. *J Mol Biol* 324:1031–1040.
35. Sridevi K, Udgaonkar JB (2002) Unfolding rates of barstar determined in native and low denaturant conditions indicate the presence of intermediates. *Biochemistry* 41:1568–1578.
36. Cliff MJ, et al. (2006) A thiol labelling competition experiment as a probe for sidechain packing in the kinetic folding intermediate of N-PGK. *J Mol Biol* 364:810–823.
37. Jha SK, Udgaonkar JB (2007) Exploring the cooperativity of the fast folding reaction of a small protein using pulsed thiol labeling and mass spectrometry. *J Biol Chem* 282:37479–37491.
38. Johnson CP, Tang HY, Carag C, Speicher DW, Discher DE (2007) Forced unfolding of proteins within cells. *Science* 317:663–666.
39. Isom DG, Vardy E, Oas TG, Hellinga HW (2010) Picomole-scale characterization of protein stability and function by quantitative cysteine reactivity. *Proc Natl Acad Sci USA* 107:4908–4913.
40. Krishnan B, Gierasch LM (2011) Dynamic local unfolding in the serpin alpha-1 antitrypsin provides a mechanism for loop insertion and polymerization. *Nat Struct Mol Biol* 18:222–226.
41. Raschke TM, Marqusee S (1997) The kinetic folding intermediate of ribonuclease H resembles the acid molten globule and partially unfolded molecules detected under native conditions. *Nat Struct Biol* 4:298–304.
42. Goedken ER, Marqusee S (2001) Native-state energetics of a thermostabilized variant of ribonuclease HI. *J Mol Biol* 314:863–871.
43. Silverman JA, Harbury PB (2002) Rapid mapping of protein structure, interactions, and ligand binding by misincorporation proton-alkyl exchange. *J Biol Chem* 277:30968–30975.
44. Raschke TM, Kho J, Marqusee S (1999) Confirmation of the hierarchical folding of RNase H: a protein engineering study. *Nat Struct Biol* 6:825–831.
45. Dabora JM, Marqusee S (1994) Equilibrium unfolding of *Escherichia coli* ribonuclease H: characterization of a partially folded state. *Protein Sci* 3:1401–1408.
46. Yin J, et al. (2005) Genetically encoded short peptide tag for versatile protein labeling by Sfp phosphopantetheinyl transferase. *Proc Natl Acad Sci USA* 102:15815–15820.
47. Xiao H, et al. (2005) Mapping protein energy landscapes with amide hydrogen exchange and mass spectrometry: I. A generalized model for a two-state protein and comparison with experiment. *Protein Sci* 14:543–557.
48. Goedken ER, Raschke TM, Marqusee S (1997) Importance of the C-terminal helix to the stability and enzymatic activity of *Escherichia coli* ribonuclease H. *Biochemistry* 36:7256–7263.
49. Hollien J, Marqusee S (1999) Structural distribution of stability in a thermophilic enzyme. *Proc Natl Acad Sci USA* 96:13674–13678.
50. Bruix M, et al. (2008) Destabilizing mutations alter the hydrogen exchange mechanism in ribonuclease A. *Biophys J* 94:2297–2305.
51. Canet D, et al. (2002) Local cooperativity in the unfolding of an amyloidogenic variant of human lysozyme. *Nat Struct Biol* 9:308–315.
52. Jha SK, Udgaonkar JB (2009) Direct evidence for a dry molten globule intermediate during the unfolding of a small protein. *Proc Natl Acad Sci USA* 106:12289–12294.
53. Stratton MM, Cutler TA, Ha JH, Loh SN (2010) Probing local structural fluctuations in myoglobin by size-dependent thiol-disulfide exchange. *Protein Sci* 19:1587–1594.